10

Atomic and electronic structure of nitrogen-doped nano-graphene clusters by combined XPS and XAFS analysis

© D.B. Tolchina[1], L.A. Avakyan[1], V.V. Srabionyan[1], H. Gyulasaryan[2], A.T. Kozakov[3], A.V. Nikolskiy[3], A.V. Emelyanov[4], R.G. Chumakov[4], E.G. Sharoyan[2], A.S. Manukyan[2], L.A. Bugaev[1,¶]

[1] Southern Federal University, Rostov-on-Don, Russia
[2] The Institute for Physical Research of National Academy of Sciences of Armenia, Ashtarak, Armenia
[3] Southern Federal University, Research Institute of Physics, Rostov-on-Don, Russia
[4] National Research Center „Kurchatov Institute“, Moscow, Russia

¶ E-mail: bugaev@sfedu.ru

Received October 31, 2023
Revised January 21, 2024
Accepted January 26, 2024

Changes in the local structure of nitrogen-containing carbon samples obtained by solid-phase pyrolysis of phthalonitrile and phthalocyanine at different pressures have been determined. The structure of carbon microspheres in the samples was studied by transmission electron microscopy. By combined analyzing the N 1*s* X-ray photoelectronic spectroscopy data (N 1*s* XPS) and fitting it with experimental N *K*-edge X-ray absorption near edge structure data (N *K*-edge XANES) the bond types and atomic structure parameters for the local structure of nitrogen in the synthesised samples have been determined. Bond lengths and angles in nitrogen-containing atomic configurations were determined, including three-atom C−N−C chains for pyridinic and pyrrolic nitrogen, as well as O=N−2C configurations for Quaternary nitrogen (QN) =Quaternary N (QN)=Oxidized N (ON). The percentage of these structural states of nitrogen in the samples and its dependence on the synthesis conditions were determined.

Keywords: nitrogen-doped nanographene clusters, solid-phase pyrolysis, XPS, XANES, nitrogen structural states, Pyridine N/Pyrrole N.

DOI: 10.61011/PSS.2024.03.57948.244

1. Introduction

Ferromagnetism of the compounds containing only the *p*- and *s*-electrons is a fast-developing scientific field [1]. The past few decades have seen a lot of experimental and theoretical studies which indicate that features of the carbon electron structure can result in development of ferromagnetic correlations kept even at the elevated temperatures [2–10]. The study [11] has shown that in case of replacing some part of carbon atoms in a graphene sheet with three-valence atoms, such as B, N, Al, then a significant magnetic moment can be formed in such a system.

The present study provides results of determination of the electron and atom structure of four carbon samples that are doped with nitrogen. The samples were synthesized by a method of solid-phase pyrolysis of phthalonitrile and phthalocyanine at different pressures. As established in [12], application of this approach allowed us to obtain the nitrogen-doped carbon samples that have stable ferromagnetic characteristics at room temperature. The present study has aimed at changing the pyrolysis conditions in order to obtain a different concentration of nitrogen containing centers and define the structure of such centers. For study of the structural features of the materials synthesized under the considered conditions, including identification of nanographene clusters in the carbon structures, we have used methods of transmission electron microscopy and scanning election microscopy (TEM, SEM) and energy-dispersive X-ray microscopy (EDX). The elementary composition and the types of chemical bonds in the materials have been determined using X-ray photoelectron spectroscopy (XPS). The atomic structure of the nitrogen centers has been determined in a combined approach used to apply the results of analysis of the N 1*s* XPS-spectra in constructing nitrogen nearest-neighbor models in the studies samples. After that, the obtained structure models were used and verified during fitting an experimental near-edge region of the nitrogen X-ray absorption spectra (N *K*-edge XANES) in each of the samples by the theoretical spectra corresponding to these models. Using this approach has helped determining the parameters of the nitrogen nearest-neighbor structure in the studied samples and changes thereof due to varying synthesis conditions.

2. Experimental and theoretical methods

2.1. Production of the samples and experimental studies

The studied samples were synthesized based on phthalocyanine ($(C_8H_4N_2)_4H_2$) and phthalonitrile ($C_8H_4N_2$), which were used as precursors to obtain carbon-based nano- and micro-spheres. The initial materials of phthalocyanine and phthalonitrile had chemical purity of the extra-pure grade, with an impurity content of 0.00001%. The solid phase pyrolysis reaction was carried out in the three-zone tube furnace in the N_2 atmosphere with a pressure control system. The pyrolysis process can be described by the following chemical reactions

$$C_{32}H_{18}N_8 \xrightarrow{\text{pyrolysis}} 32C + 9H_2 + 4N_2, \quad (1)$$

$$C_8H_4N_2 \xrightarrow{\text{pyrolysis}} 8C + 2H_2 + N_2. \quad (2)$$

The pyrolysis was conducted at constant temperature of 700°C for 30 min at various pressures in the heating tube. The samples PN-0 and PN-15 were obtained by phthalonitrile pyrolysis at the pressures of 0.01 and 15.0 bar, respectively, while the sample PC-0 was obtained by pyrolysis of phthalonitrile at the pressure of 0.01 bar inside the reactor. In order to investigate interrelation between the synthesis conditions and the structural characteristics of the sample, this set was supplemented by the sample PC-1 obtained at the pressure of 1 bar in the study [12].

The size, form and elementary composition of the spheres were studied by the SEM, TEM and EDX methods in the electron microscope JEM-F200 (JEOL) designed to operate at an accelerating voltage of 200 kV. The EDX-analysis was done by means of the system Bruker Xflash 6T/60 Quantax 400-STEM with 4000 channels, including the energy-dispersive detector XFlash having a thickness of 0.45 mm and an operating temperature of −25°C. The elemental mapping was performed at the primary energy of 200 kV within the energy range 10−20 eV with the total measurement time of 10 min.

The XPS-studies of the powder samples were performed at the room temperature in the X-ray photoelectron microprobe ESCALAB 250. The samples were pre-applied to a double-side adhesive conducting tape. The samples were excited with monochromatic AlK_α-radiation. The XPS-spectra of C 1*s*, N 1*s*, O 1*s* were recorded as excited by the AlK_α-line. The absolute energy resolution was 0.6 eV, which was determined from the profile of the Ag $3d_{5/2}$ line. The diameter of the X-ray spot on the sample surface was 500 μm.

The X-ray absorption N *K*-XANES-spectrum were measured at the NanoPES experimental station of the Kurchatov Synchrotron Radiation source [13]. All the spectra were measured in a full-electron yield mode with the energy resolution dE/E not exceeding 0.2 eV and at thesize $100 \times 300\,\mu m^2$.

2.2. Theoretical methods and approaches

The N *K*-XANES-spectrum were calculated using a full potential and finite differences method implemented in the software package FDMNES [14]. In order to establish the N *K*-XANES describability in the studied samples by means of FDMNES, the spectra were calculated for the reference sample of phthalocyanine ($(C_8H_4N_2)_4H_2$). The experimental spectra of $(C_8H_4N_2)_4H_2$ measured for the two directions of polarization of incident radiation (30 and 90°) [15] were compared with the respective theoretical spectra calculated using the Hedin-Lundqvist's exchange-correlation potential to show good quantitative agreement. The theoretical N *K*-XANES-spectrum were quantitatively compared with the experimental ones using values of a discrepancy parameter χ^2 [16].

3. Results and discussion

3.1. Analysis of TEM-images

The SEM-images (Figure 1, *a, b*) confirm formation of the microscope spheres in the studied samples. The spheres have a homogeneous structure and an average size about 2 μm (the size and the size dispersion $2.5 \pm 0.4\,\mu$m and $1.8 \pm 0.6\,\mu$m for the samples PN-0 and PN-15, respectively). Figure 1, *c* shows the image of a section of the sample PC-0, whose appearance is typical for other samples under study. The TEM-images show a dense internal structure of the samples, while EDX-elemental mapping indicates that the spheres predominantly consist of carbon (Figure 1, *d*). As expected, the samples have nitrogen (Figure 1, *e*) that is uniformly distributed across the carbon sphere. Apparently, presence of oxygen (Figure 1, *f*) is related to oxidation of the sample after pyrolysis.

3.2. Investigation of the samples in the XPS method

The reviewed XPS spectra were analyzed to show that they exhibited no other lines except for O 1*s*-, C 1*s*- and N 1*s*-peaks relating to carbon, nitrogen and oxygen, respectively. Hydrogen can contribute to the intensity of these lines only when being in a composition of separate functional groups. So, the elemental sample composition of Table 1 actually contains the number of the atoms of

Table 1. Designations and the elemental composition of the samples

Sample	Pressure in the autoclave, bar	Elemental composition, at.%		
		C	N	O
PN-0	0.01	79.8	16.8	3.4
PN-15	15	82.9	11.0	6.1
PC-0	0.01	80.2	14.6	5.2
PC-1	1	80.0	7.3	12.7

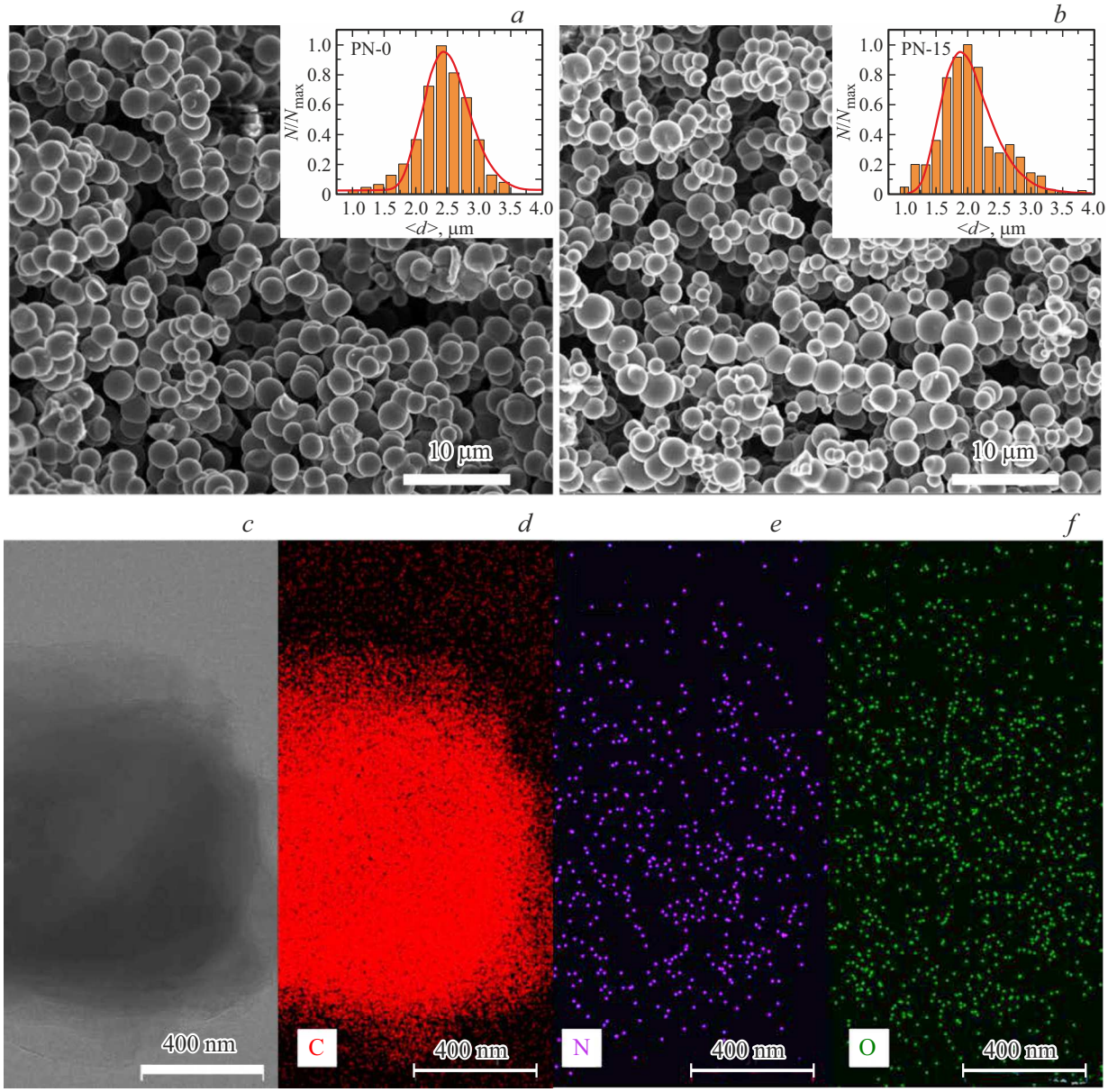

Figure 1. SEM-images of the samples PN-0 (*a*), PN-15 (*b*), TEM-image of the sample PC-0 (*c*) and its respective EDX-elemental mapping of the atoms of (*d*), nitrogen (*e*) and oxygen (*f*).

oxygen, carbon and nitrogen which is less by the amount of the atoms of hydrogen inside the functional groups bound by oxygen, carbon and nitrogen. Table 1 also shows the used designations of the samples and the pressures of nitrogen atmosphere in the autoclave, which correspond thereto.

3.3. N 1*s* XPS

Figure 2 shows the decompositions of the N 1s XPS-spectra to the components. The energies of such components in the performed decompositions are shown in Table 2. Due to a large number of possible various types of the local environments of the embedded atoms of nitrogen, their bond energies of the nearest neighbors can noticeably vary in the samples. Therefore, Table 2 shows the energy ranges for the components that were identified for classification as per a bond type in accordance with the data of the studies [17–24]

We relate the component *A* with the energy varying within the range 398.3–399.0 eV to Pyridinic N, when nitrogen occupies vacancies between two carbon atomsthe graphene layer on at the edge thereof — the graphene plane or on its edge [17,18,20–22]. The study [25] relates the component with the energy of 399.0 eV in the decomposition of N 1s XPS to nitrogen in the nitrile group $CH_3-C{=}N$ in ethanenitrile with three atoms of hydrogen or in formonitrile with one atom of hydrogen.

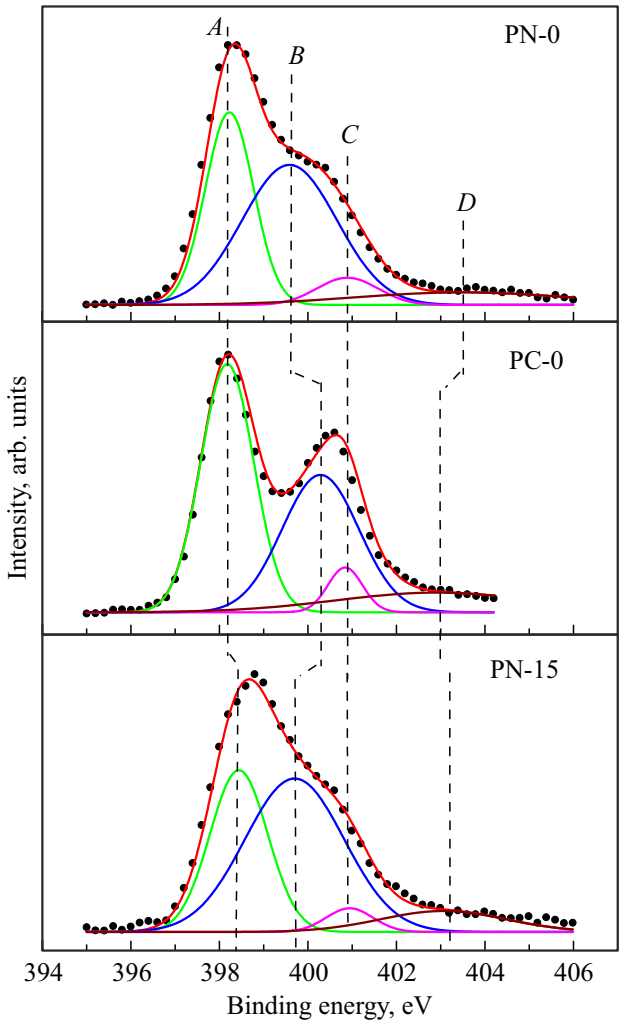

Figure 2. Decomposition of N 1*s* XPS to the components for the samples: *1* — PN-0, *2* — PC-0, *3* — PN-15.

In order to identify the component *B*, we have broadened the energy range from 399.3 to 400.4 eV. It can relate this component not only to the simple case of Pyrrolic N (i.e. the nitrogen atom with the energy of 1*s* within the range 399.5–400 eV), arranged in a five-member ring [17–19,22], but to more complex pyrrolic configurations, such as tertiary N in the form of $N-(C)_3$ or $H-N-(C)_2$ [24].

The component *C* with the energy of 400.4–401.1 eV, in accordance with [22], is ascribed to such a structure of Pyridinic N, for which the atom of carbon is not only replaced by the atom of nitrogen at the vertex of the six-membered ring, but at the same time the OH group is attached to one of the neighbor atoms of carbon. The component *C* must have the same energy (400.7 eV), if the sample contains nitrogen in the functional groups C–N=O or N–Q [24], i. e. it contains quaternary- coordinated nitrogen (Quaternary N (QN) or Oxidized N) in pyridinic and/or ammonium compounds between the graphene planes [22]. The relative high intensity of *C* can be caused either by a high number of the groups OH in the samples, or the high number of the functional groups bonded by nitrogen, i. e. the groups C–N=O. The atoms of oxygen inside the functional groups are not directly related to the atoms of carbon.

The high-energy component *D* has a relatively weak intensity for XPS of all the samples. As per [18–20,22], it can be related to graphitic N, and as per [23], the same energy range includes a component of the N 1*s* of the spectrum related to quaternary amines $(N(CH_3)_3^+)$.

3.4. Analysis of the N *K*-edge XANES based on the N 1*s* XPS results

The analysis-obtained N 1*s* XPS data of Table 2 indicate a variety and ambiguity of nitrogen bonds or structural states in the studied samples. In order to remove these unambiguities, detect the nitrogen bonds available in the samples and to determine structural parameters of these bonds, the N *K*-XANES-spectrum of the samples have been analyzed. Figure 3 shows comparison of the experimental N *K*-XANES-spectrum of the samples under study, which demonstrate noticeable sensitivity of a fine structure of the spectra both to selection of the precursor and the synthesis conditions. At the same time, if the fine structure of the spectra within the energy range 395–402 eV (the peaks *A*–*D*), ascribed to the unoccupied π-orbitals [26], is very sensitive to the synthesis conditions, while the broad feature at $\sim$ 406 eV, ascribed to the σ-states [26], is less sensitive.

As noted above, it follows from the XPS data of Table 2 that the atoms of nitrogen in each sample have a different structural environment with higher probability. As a result, it can be expected that the observed N *K*-XANES-spectrum is formed as a sum of contributions of the different possible structure states of the absorbing N atom in the sample. Despite the high sensitivity of the XANES-spectrum to

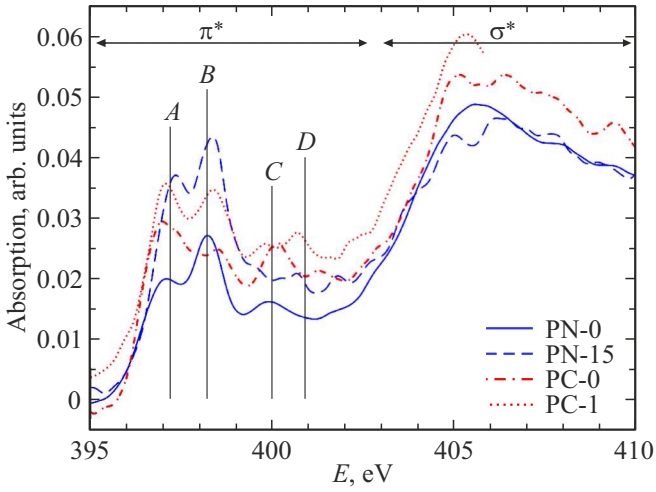

Figure 3. Experimental N *K*-XANES-spectrum of the samples: PN-0 — the solid blue curve, PN-15 — the dashed blue curve, PC-0 — the dash-dotted curve, PC-1 — the dashed red curve.

Table 2. Energy position (eV) of the components in decomposition of the N 1*s* XPS-spectra of the samples PN-0, PN-15, PC-0, PC-1

Sample	Energies of the components in the spectrum N 1*s* XPS (eV)			
	A Pyridinic N	*B* Pyrrolic N	*C* Quaternery N, Oxydised N	*D* Graphitic N
	398.3–399.0	399.3–400.3	400.4–401.1	402.1–403.6
PN-0	398.3	399.8	400.8	403
PN-15	398.9	400.0	400.9	402.7
PC-0	398.3	399.4	400.5	401.8
PC-1	398.45	399.6	400.8	401.75

the features of the radial and angular distributions of the nearest neighbors of the absorbing atoms [27–29], heavy amorphization of the initial structures PC and PN during the solid-phase pyrolysis has made it possible to expect that the experimental spectrum could be theoretically described as a sum of the contributions of several different atomic configurations for the nitrogen environment, as proposed by Table 2, which includes only the nearest neighbors of the absorbing N. At the same time, it is obvious that for the first one of such N structure states, it is reasonable to consider the contribution of the simplest, but the most probable atomic configuration that consists of the absorbing atom of N connected with the two nearest neighbor atoms of C (the three-atom chain C–N–C). This atomic configuration C–N–C is present in almost all main components of decomposition of the N 1*s* XPS-spectra of Table 2, since it can be related to different crystallographic carbon structures —pyridinic, pyrrolic, graphite ones that differ by the lengths ($R_{\mathrm{N-C}}$) and the angles of the bonds ($\alpha_{\mathrm{C-N-C}}$ at the vertex N).

The contributions of the chains of C–N–C in N *K*-XANES were calculated to show that the energy position and the relative intensities of the spectral features *A*, *B* within the energy range 395–399 eV of the spectra of Figure 3 are very sensitive to a structural geometry of the atom chains C–N–C. Such sensitivity could determine the structural parameters of the chains in consideration by locally fitting the experimental N *K*-XANES-spectrum by the theoretical contributions calculated for the different C–N–C chains with the widely-varied lengths and angles of the bonds. Figure 4 compares the experimental N *K*-XANES and theoretical spectra in the sample PN-0, as calculated for the atom chains C–N–C, with the two different sets, as obtained from the fitting, of the interatomic distances $R_{\mathrm{N-C}}$ and the angles of the bonds $\alpha_{\mathrm{C-N-C}}$: the first set of $R_{\mathrm{N-C}} = 1.48$ Å and $\alpha_{\mathrm{C-N-C}} \sim 118^\circ$ (which turned out to be typical for Pyridinic N, Figure 4, *a*) and the second set with $R_{\mathrm{N-C}} = 1.43$ Å and $\alpha_{\mathrm{C-N-C}} \sim 105^\circ$ (which is typical for Pyrrolic N, Figure 4, *b*). The comparison of Figure 4, *a* shows that the considered chain C–N–C with the parameters of the pyridinic structure can reproduce a single peak *A* in N *K*-XANES, which also agrees with the experimental spectrum of pyridine in aqueous solution [30]. The comparison of Figure 4, *b* shows that the second peak *B* in N *K*-XANES is caused by the contribution of Pyrrolic N. Another important result for structural analysis of the samples of the studied class is both energy separation of the peaks *A*, *B* from each other (at ~ 1 eV) and their significant spacing from the next wide peak *E* that is usually related to the contribution of the unoccupied σ-orbitals.

The experimental features *A*, *B* have been compared on Figure 4, *a, b* with the calculated ones so as to assume that these peak in the experimental spectrum could be reproduced by the sum of at least two different structural configurations of the chains C–N–C with the partial weights C_i, whose first configuration of the chain corresponds to the Pyridinic N state in the sample, so does the second one — to Pyrrolic N, which agrees with the XPS data. The calculations have been performed to show that the physically justified variations of the lengths $R_{\mathrm{N-C}}$ and the angles of the bonds $\alpha_{\mathrm{C-N-C}}$ within the model of the framework of the N nearest neighbor local structure that consisted only of the chains of the type C–N–C, were insufficient for reproducing the features of C and D in the N *K*-XANES-spectrum within the energy range 399–402 eV (Figure 3).

So, in order to implement the N nearest-neighbor structural analysis in the samples by using the entire energy region of the N *K*-XANES-spectrum, the following approach has been realized to check the atom models of the local structure around nitrogen as proposed by the data of analysis of N 1*s* XPS and to determine the respective structural parameters, based on theoretical description and fitting of the experimental N *K*-XANES-spectrum of the sample by these models. In accordance with this approach, the experimental spectrum was fit by the sum of the calculated contributions from particular types of the N local structure, as proposed by the data of analysis of N 1*s* XPS from Table 2. The fitting resulted in determination of the values of the parameters for each N structure state: the lengths and the angles of the bonds, the percent content of C_i and the energy shift of the ε_i *i*-th N structure state in total. It should be noted that the obtained values of the

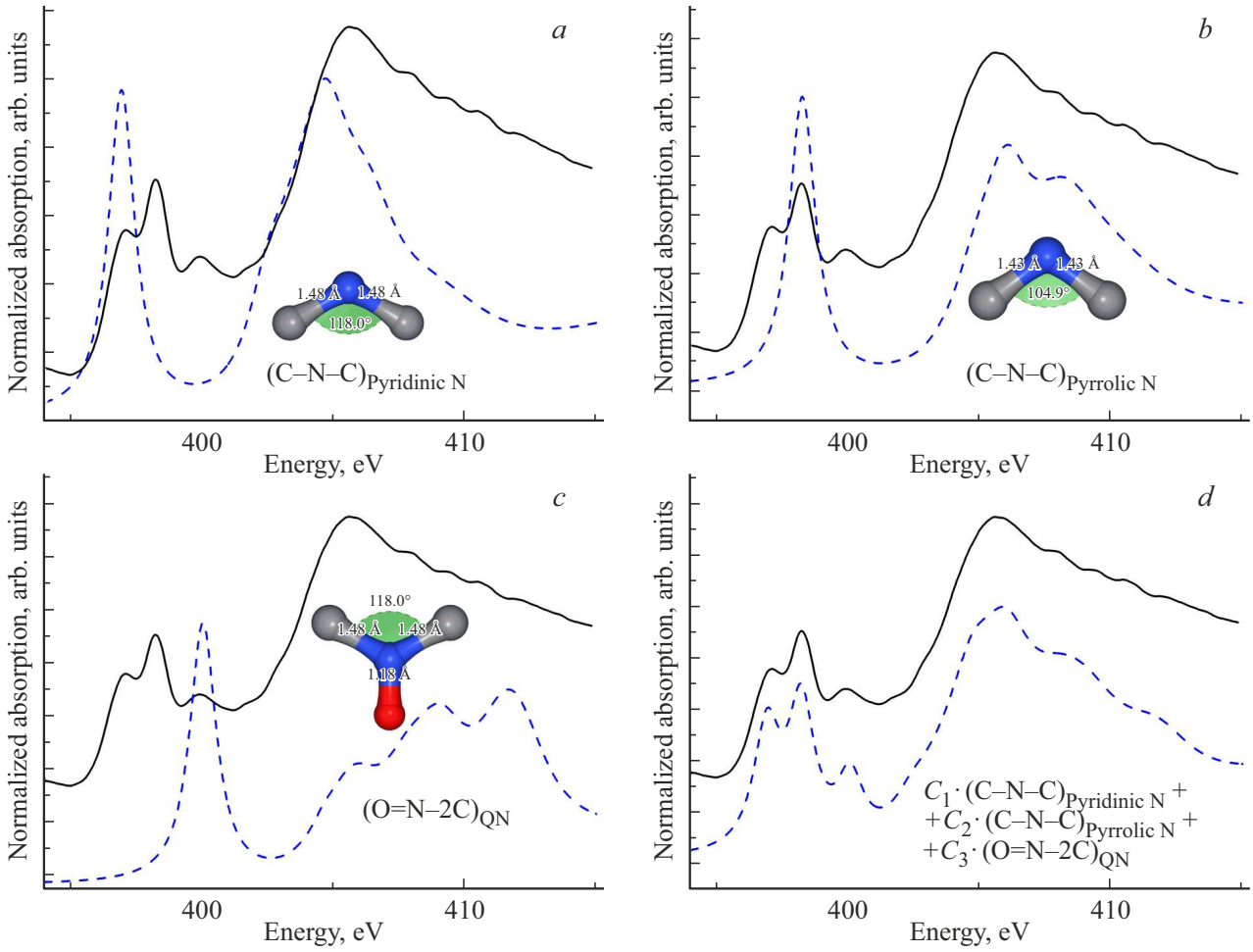

Figure 4. Comparison of the experimental N *K*-XANES-spectrum (the solid blackline) in the sample PN-0 and the theoretical spectra (the dashed blue lines), as calculated for: *a* — the atom chain $(C{-}N{-}C)_{\text{Pyridinic N}}$ with $R_{N-C} = 1.48$ Å, $\alpha_{C-N-C} \sim 118°$, typical for Pyridinic N; *b* — the atom chain $(C{-}N{-}C)_{\text{Pyridinic N}}$ with $R_{N-C} = 1.43$ Å, $\alpha_{C-N-C} \sim 105°$, typical for Pyrrolic N; *c* — the atom chain $(0{=}N{-}2C)_{NQ}$ with $R_{N-O} = 1.18$ Å, $R_{N-C} = 1.48$ Å, $\alpha_{C-N-C} \sim 118°$ typical for the four-coordinated N; *d* — the sum of the three contributions: $C_1^*(C{-}N{-}C)_{\text{Pyridinic N}} + C_2^*(C{-}N{-}C)_{\text{Pyrrolic N}} + C_3^*(O{=}N{-}2C)_{QN}$.

energy shifts ε_i were checked by comparing the differences $(\varepsilon_i - \varepsilon_j)$ with the same differences of the energy bond of the N 1*s*-levels in the respective atom configurations as available in the XPS data. The best model of the nitrogen nearest-neighbor structure was selected by the results of fitting by means of the discrepancy values χ^2 calculated in accordance with [27].

Figure 4, *d* compares the experimental N *K*-XANES for the sample PN-0 with the theoretical spectrum calculated as the sum of the contributions of the three structure states of the N atoms in the sample, as proposed as per the results of the N 1*s* XPS analysis of Table 2: the atom chain C−N−C Pyridinic N (the chain $(C{-}N{-}C)_{\text{PyridinicN}}$ of Figure 4, *a*) with the percentage ratio $C_1 = 0.39\%$, the atom chain C−N−C Pyrrolic N (the chain $(C{-}N{-}C)_{\text{PyridinicN}}$ of Figure 4, *b*) with the percent ratio $C_2 = 0.43\%$ and the atom configuration O=N−2C of the four-coordinated or oxidized N (the configuration $(O{=}N{-}2C)_{\text{QuaternaryN}}$), as shown on Figure 4, *c* with the structure parameters as obtained from the fitting

$$R_{N-O} = 1.18\,\text{Å}, \quad R_{N-C} = 1.48\,\text{Å},$$

$$R_{N-O} = 1.45\,\text{Å}, \quad \alpha_{C-N-C} \sim 118° \text{ and } C_3 = 0.18\%.$$

Let us note that the satisfactorily compliance of the experimental and theoretical spectra N *K*-XANES within the energy range 403−410 eV (the feature *E* of Figure 4, *d*), which is reproduced for the various values of the distances R_{N-C} and the angles α_{C-N-C} (Figure 4, *a*−*c*), can make it to conclude that the electron structure of the unoccupied σ-orbitals in the studied samples is mainly formed by the bonds C−N in the simplest three-atom chains C−N−C with the bond lengths R_{N-C} and the bond angels α_{C-N-C}, which are typical for pyridinic and pyrrolic nitrogen.

Table 3 shows the values of the ratio (Pyridinic N/Pyrrolic N), which are obtained from fitting the experimental N *K*-XANES of the studied samples, as based

Table 3. Values of the ratio (Pyridinic N)/(Pyrrolic N) together with the percent content of the main structure states of nitrogen in the studied samples, as obtained from the fitting of the experimental N *K*-XANES-spectrum of the samples by the theoretical contributions that are calculated based on the established structure states of nitrogen

Sample	Ratio (Pyridinic N)/(Pyrrolic N) and the percentage rations of the main structure states of N in the samples
PN-0	(Pyridinic N)/(Pyrrolic N) = 0.91 Pyridinic N = 0.39 Pyrrolic N = 0.43 four-coordinated N (QN) Oxydized N = 0.18
PN-15	(Pyridinic N)/(Pyrrolic N) = 0.55 Pyridinic N = 0.29 Pyrrolic N = 0.53 four-coordinated N (QN) Oxydized N = 0.18
PC-0	(Pyridinic N)/(Pyrrolic N) = 1.27 Pyridinic N = 0.39 Pyrrolic N = 0.30 four-coordinated N (QN) Oxydized N = 0.31
PC-1	(Pyridinic N)/(Pyrrolic N) = 1.01 Pyridinic N = 0.35 Pyrrolic N = 0.35 four-coordinated N (QN) Oxydized N = 0.27

on the nitrogen nearest neighbor model consisting of superposition of the three above-determined contributions: $C_1^*(\mathrm{C{-}N{-}C})_{\mathrm{Pyridinic\,N}} + C_2^*(\mathrm{C{-}N{-}C})_{\mathrm{Pyrrolic\,N}} + +C_3^*(\mathrm{O{=}N{-}2C})_{\mathrm{QN}}$.

4. Conclusion

The results of the performed research allow us to make the following main conclusions:

– subsequent application of analysis of the N 1*s* XPS proposing possible types of the N atom bonds in the sample, and the direct calculations of the N *K*-XANES based on the identified bonds is an effective approach that could determine the nearest-neighbor structure of the nitrogen atoms that are in different structure states in the studied sample;

– the spectrum features within the region 395–402 eV in N *K*-XANES, which are related to the contributions of the unoccupied π-orbitals, are very sensitive to the pyrolysis conditions of the studied samples (selection of an initial precursor, a chamber pressure) and mainly caused by the contributions of the three-atom configurations C–N–C with the structure parameters of pyridinic and pyrrolic nitrogen, which are components of the respective rings. The spectrum features in the energy region above 403 eV in N *K*-XANES, which are ascribed to the contributions of the unoccupied σ-orbitals are resulted from a sum of the contributions of the two types of the three-atom configurations C–N–C, which correspond to pyridinic and pyrrolic nitrogen, and the contribution of the four-atom configuration O=N–2C (four-coordinated N);

– the established energy separation of the two first edge peaks in N *K*-XANES of pyridinic and pyrrolic nitrogen has provided stability and unambiguity of the fitting of the experimental spectra, there by determining the lengths and the angles of the bonds in the three-atom C–N–C and the four-atom O=N–2C configurations, and determining the percentage ratios of these nitrogen structure states in the samples. The latter have shown a decreased fraction of pyridinic nitrogen and an increased fraction of pyrrolic nitrogen in the samples, with increase in the chamber pressure.

Funding

The study was supported by an RFBR project of and the Committee of Science of RA within the joint scientific project RFBR 20-52-05011 Arm_a and SCS 20RF-166, respectively.

Acknowledgments

The authors would like to thank Join Access Center „Modern microscopy“ of the Southern Federal University (A.A. Tsturyan and I.A. Pankov) for assistance in measurement and interpretation of the TEM-spectra o the samples. A.T. Kozakov and A.V. Nikol'skii would like to thank the Ministry of Science and Higher Education of the Russian Federation (State assignment in the field of scientific acitivity 2023 No. FENW-2023-0014) for financial support of the studies.

Conflict of interest

The authors declare that they have no conflict of interest.

References

[1] J.S. Miller, M. Drillon. Magnetism: Molecules to Materials (2005). V. 1.
[2] V.V. Korolev, T.N. Lomova, A.G. Ramazanova. Radioelectron. Nanosystems. Inform. Technologies **11**, 199 (2019).
[3] P. Esquinazi, A. Setzer, R. Höhne, C. Semmelhack, Y. Kopelevich, D. Spemann, T. Butz, B. Kohlstrunk, M. Lösche. Phys. Rev. B **66**, 024429 (2002).
[4] S. Talapatra, P.G. Ganesan, T. Kim, R. Vajtai, M. Huang, M. Shima, G. Ramanath, D. Srivastava, S.C. Deevi, P.M. Ajayan. Phys. Rev. Lett. **95**, 097201 (2005).
[5] X. Yang, H. Xia, X. Qin, W. Li, Y. Dai, X. Liu, M. Zhao, Y. Xia, S. Yan, B. Wang. Carbon N.Y. **47**, 1399 (2009).

[6] A.L. Friedman, H. Chun, Y.J. Jung, D. Heiman, E.R. Glaser, L. Menon. Phys. Rev. B Condens. Matter Mater. Phys. **81**, 115461 (2010).
[7] Y. Liu, N. Tang, X. Wan, Q. Feng, M. Li, Q. Xu, F. Liu, Y. Du. Sci. Rep. **3**, 1 (2013).
[8] D. Gao, Y. Liu, M. Song, S. Shi, M. Si, D. Xue. J. Mater. Chem. C **3**, 12230 (2015).
[9] X. Zhou, F. Li, Y. Xing, W. Feng. J. Mater. Chem. C **7**, 3360 (2019).
[10] L. Du, B. Gao, S. Xu, Q. Xu. Nature Commun. **14**, 1 (2023).
[11] A.A. Ovchinnikov, V.N. Spector. Synth Met. **27**, 615 (1988).
[12] A. Manukyan, H. Gyulasaryan, A. Kocharian, P. Oyala, R. Chumakov, M. Avramenko, C. Sanchez, O.O. Bernal, L. Bugaev, E. Sharoyan. J. Phys. Chem. C **126**, 493 (2022).
[13] A.M. Lebedev, K.A. Menshikov, V.G. Nazin, V.G. Stankevich, M.B. Tsetlin, R.G. Chumakov. J. Surface Investigation: X-Ray, Synchrotron Neutron Techniques **15**, 1039 (2021).
[14] Y. Joly. Phys Rev. B **63**, 125120 (2001).
[15] T.M. Willey, M. Bagge-Hansen, J.R.I. Lee, R. Call, L. Landt, T. Van Buuren, C. Colesniuc, C. Monton, I. Valmianski, I.K. Schuller. J. Chem. Phys. **139**, (2013).
[16] https://cars.uchicago.edu/ifeffit/.
[17] S.N. Nesov, P.M. Korusenko, V.V. Bolotov, S.N. Povoroznyuk, D.A. Smirnov. FTT **59**, 2006 (2017). (in Russian).
[18] H. Wang, T. Maiyalagan, X. Wang, ACS Catal. **2**, 781 (2012).
[19] J. Li, X. Li, P. Zhao, D.Y. Lei, W. Li, J. Bai, Z. Ren, X. Xu. Carbon (N.Y.) **84**, 460 (2015).
[20] Q. Miao, L. Wang, Z. Liu, B. Wei, F. Xu, W. Fei. Sci. Rep. **6**, 1 (2016).
[21] X. Li, H. Wang, J.T. Robinson, H. Sanchez, G. Diankov, H. Dai. J. Am. Chem. Soc. **131**, 15939 (2009).
[22] C. Weidenthaler, A.H. Lu, W. Schmidt, F. Schüth. Micropor. Mesopor. Mater. **88**, 238 (2006).
[23] K. Artyushkova, S. Levendosky, P. Atanassov, J. Fulghum. Top Catal. **46**, 263 (2007).
[24] L.F. Chen, X.D. Zhang, H.W. Liang, M. Kong, Q.F. Guan, P. Chen, Z.Y. Wu, S.H. Yu. ACS Nano **6**, 7092 (2012).
[25] R. Ohta, K.H. Lee, N. Saito, Y. Inoue, H. Sugimura, O. Takai. Thin Solid Films **434**, 296 (2003).
[26] K.G. Latham, M.I. Simone, W.M. Dose, J.A. Allen, S.W. Donne. Carbon (N.Y.) **114**, 566 (2017).
[27] V.V. Srabionyan, G.B. Sukharina, T.I. Kurzina, V.A. Durymanov, A.M. Ermakova, L.A. Avakyan, E.M.C. Alayon, M. Nachtegaal, J.A. Van Bokhoven, L.A. Bugaev. J. Phys. Chem. C **125**, 25867 (2021).
[28] V.V. Srabionyan, L.A. Avakyan, V.A. Durymanov, D.S. Rubanik, I.A. Viklenko, A.V. Skunova, L.A. Bugaev. J. Phys. Chem. Solids **179**, 111412 (2023).
[29] J.A. van Bokhoven, C. Lamberti. X-ray absorption and X-ray emission spectroscopy: theory and applications. https://www.wiley.com/en-ie/X+Ray+Absorption+and+X+Ray+Emission+Spectroscopy3A+Theory+and+Applications-p-9781118844236 (accessed May 7, 2023).
[30] M. Nagasaka, H. Yuzawa, N. Kosugi. Z. Physikalische Chem. **232**, 705 (2018).

Translated by M.Shevelev